arXiv:2308.01303v1 [hep-lat] 2 Aug 2023

The chiral condensate of $N_f = 2+1$ QCD from the spectrum of the staggered Dirac operator

Claudio Bonanno,[a] **Francesco D'Angelo**[b] **and Massimo D'Elia**[b]

[a]*Instituto de Física Teórica UAM-CSIC, c/ Nicolás Cabrera 13-15, Universidad Autónoma de Madrid, Cantoblanco, E-28049 Madrid, Spain*

[b]*Università di Pisa and INFN Sezione di Pisa, Largo B. Pontecorvo 3, I-56127 Pisa, Italy*

E-mail: claudio.bonanno@csic.es, francesco.dangelo@phd.unipi.it, massimo.delia@unipi.it

ABSTRACT: We compute the chiral condensate of $2+1$ QCD from the mode number of the staggered Dirac operator, performing controlled extrapolations to both the continuum and the chiral limit. We consider also alternative strategies, based on the quark mass dependence of the topological susceptibility and of the pion mass, and obtain consistent results within errors. Results are also consistent with phenomenological expectations and with previous numerical determinations obtained with different lattice discretizations.

Contents

1 Introduction

Flavor symmetries in QCD and their realization play a key role in determining the most relevant theoretical non-perturbative features of the theory, as well as being linked to several interesting phenomenological aspects of strong interactions. In this respect, Chiral Perturbation Theory [1, 2] (ChPT) is able to provide remarkably accurate qualitative and quantitative predictions about QCD from an effective Lagrangian essentially built over the salient properties of the chiral symmetry exhibited by the full theory, once a few Low Energy Constants (LECs), not computable within the effective theory alone, are fixed. A possible way to fix them is to match ChPT predictions with experimentally measurable quantities (such as hadron masses). Another, more theoretically driven, strategy is to match such quantities with observables of the full theory, and to compute them non-perturbatively from first-principles methods, such as lattice Monte Carlo simulations.

At Leading Order (LO) of the chiral expansion, and considering only two light quark flavors (u, d), only two LECs are needed to fully specify the SU(2) effective theory, the chiral condensate Σ and the pion decay constant F_π:

$$\Sigma \equiv - \lim_{m_u, m_d \to 0} \langle \overline{u} u \rangle \,, \tag{1.1}$$

$$F_\pi \equiv \lim_{m_u, m_d \to 0} \frac{1}{M_\pi} \langle \Omega | \, \overline{u} \gamma_4 \gamma_5 d \, | \pi(\vec{p} = \vec{0}) \rangle \,, \tag{1.2}$$

where M_π is the pion mass, and u and d represent, respectively, the spinors of the up and down quarks.

Phenomenological estimates can be obtained combining experimental results and theoretical ChPT predictions, in particular the well-known Gell-Mann–Oakes–Renner (GMOR) relation, which, at LO in ChPT with 2 light flavors, reads:

$$M_\pi^2 = \frac{\Sigma}{F_\pi^2}(m_u + m_d). \tag{1.3}$$

The PDG [3] reports: $M_\pi = 134.9768(5)$ MeV, $F_\pi^{(\text{phys})} = 92.28(11)$ MeV[1], $m_u^{(\text{phys})} = 2.16(49)$ MeV and $m_d^{(\text{phys})} = 4.67(48)$ MeV, leading to $\Sigma_{\text{pheno}} = [283(24)\text{ MeV}]^3$. Although such estimation is done using the pion decay constant at the physical point, while the GMOR relation involves the pion decay constant in the chiral limit, cf. Eq. (1.2), this number turns out to be in perfect agreement with lattice calculations, as we will discuss in the following. This can be viewed as a confirmation of the main hypothesis underlying ChPT, i.e., that the u and d quark masses are sufficiently light to be treated as a small perturbation of the massless theory.

Generally speaking, chiral symmetry is a delicate issue from the viewpoint of lattice simulations. As a matter of fact, on one hand, chiral-symmetry preserving fermionic discretizations, such as Domain Wall or Overlap, are extremely computationally demanding, especially for a calculation targeting a few percent accuracy. On the other hand, the most typically employed quark discretizations, namely Wilson and staggered quarks, are computationally cheaper but explicitly break, either completely or partially, the chiral symmetry, which is recovered only in the continuum limit. This issue can introduce non-trivial numerical challenges, as it is well known, e.g., from lattice calculations of the topological susceptibility, where explicit chiral symmetry breaking and the absence of exact zero modes of the Dirac operator are the dominant sources of lattice artifacts [4–10].

Despite such issues, however, in the last ten years many lattice determinations adopting both chiral and non-chiral quarks of these and other QCD LECs have appeared in the literature, both for 2 [11–14], 2 + 1 [15–20] and even 2 + 1 + 1 quark flavors [8, 12] (see also Refs. [21–24] for numerical estimates of QCD LECs in the large-N_c limit). Predictions have been continuously refined over the time, finding overall a remarkably good agreement at the percent level among determinations obtained with a variety of lattice discretizations and numerical methods [25].

This paper can be placed within this context, as it deals with the problem of accurately determining QCD LECs on the lattice. In particular, we present an extensive calculation of the SU(2) chiral condensate in 2 + 1 QCD using staggered quarks, combining 3 different strategies, and performing controlled continuum and chiral extrapolations. To this end, we will exploit results obtained from simulations performed at 4 values of the lattice spacing, ranging from ~ 0.15 to ~ 0.07 fm, and considering 4 different lines of constant physics, corresponding to 4 values of the pseudo-Goldstone pion mass ranging from $m_\pi^{(\text{phys})}$ to $3m_\pi^{(\text{phys})}$, with the strange quark mass kept fixed at the physical point for all ensembles.

---

[1]In this work we follow the convention which yields $F_\pi = F_\pi^{(\text{phys})} \simeq 92$ MeV at the physical point. Other authors adopt the equivalent convention $f_\pi = \sqrt{2}F_\pi$, leading to $f_\pi^{(\text{phys})} \simeq 130$ MeV.

Concerning the numerical strategies pursued in this work, the main one will rely on the Giusti–Lüscher method to extract the chiral condensate from the mode number of the Dirac operator [26, 27], which is implemented and applied to the case of staggered quarks for the first time in this paper. Another method consists in extracting the chiral condensate from the quark mass dependence of the topological susceptibility. Finally, we will also check consistency with the more standard and well-established method relying on the quark mass dependence of the pion mass, which, in the case of staggered quarks, has been already employed in Ref. [16] to determine Σ.

This manuscript is organized as follows. In Sec. 2 we present our numerical setup. In Sec. 3 we present our continuum and chiral extrapolated results for the chiral condensate from the 3 different and complementary strategies outlined above. Finally, in Sec. 4 we draw our conclusions.

2 Numerical setup

In the first part of this Section we illustrate the discretization of $N_f = 2 + 1$ QCD on different Lines of Constant Physics (LCPs) adopted in our study. Then we move to a detailed discussion of the three numerical strategies exploited for the determination of the chiral condensate.

2.1 Lattice action and determination of LCPs

We perform simulations of $N_f = 2 + 1$ QCD discretized on N_s^4 hypercubic lattices with two degenerate light quark flavors $u = d = l$, with bare mass $m_u = m_d \equiv m_l$, and a strange quark flavor s with bare mass m_s. We adopt rooted stout staggered discretization of the Dirac operator:

$$\mathcal{M}_f^{(\text{stag})}[U] \equiv D_{\text{stag}}[U^{(2)}] + am_f \,,$$

$$D_{\text{stag}}[U^{(2)}] = \sum_{\mu=1}^{4} \eta_\mu(x) \left[U_\mu^{(2)}(x)\delta_{x,y-\hat{\mu}} - U_\mu^{(2)\dagger}(x - a\hat{\mu})\delta_{x,y+\hat{\mu}} \right] \,, \tag{2.1}$$

$$\eta_\mu(x) = (-1)^{x_1 + \dots + x_{\mu-1}} \,,$$

where $U_\mu^{(2)}(x)$ are the gauge links after two steps of isotropic stout smearing with $\rho_{\text{stout}} = 0.15$ [28]. The gauge sector is instead discretized by using the tree-level Symanzik-improved action:

$$S_{\text{YM}}^{(L)}[U] = -\frac{\beta}{3} \sum_{x,\mu\neq\nu} \left\{ \frac{5}{6}\Re\text{Tr}\left[\Pi_{\mu\nu}^{(1\times1)}(x) \right] - \frac{1}{12}\Re\text{Tr}\left[\Pi_{\mu\nu}^{(1\times2)}(x) \right] \right\} \,, \tag{2.2}$$

where $\Pi_{\mu\nu}^{(n\times m)}(x)$ stands for the product of non-stouted links along $n \times m$ rectangular paths, starting in the point x and extending in the (μ, ν) plane. In the end, the partition function on the lattice can be written in the following way:

$$Z_{\text{LQCD}} = \int [dU]e^{-S_{\text{YM}}^{(L)}[U]} \det\left\{ \mathcal{M}_l^{(\text{stag})}[U] \right\}^{\frac{1}{2}} \det\left\{ \mathcal{M}_s^{(\text{stag})}[U] \right\}^{\frac{1}{4}} \,. \tag{2.3}$$

The sampling of the functional integral was performed by means of the standard Rational Hybrid Monte Carlo (RHMC) algorithm [29, 30].

In order to compute the SU(2) chiral condensate, one has to take the chiral limit $m_l \to 0$ at fixed physical strange quark mass. To this end, we need to determine LCPs corresponding to different values of m_l and fixed $m_s = m_s^{(\mathrm{phys})}$.

Our starting point is the LCP with $m_l = m_l^{(\mathrm{phys})}$ (i.e., corresponding to the physical value of the pion mass $M_\pi^{(\mathrm{phys})} \simeq 135$ MeV) and with $R \equiv m_l/m_s = R^{(\mathrm{phys})} \simeq 1/28.15$, that was determined in Refs. [31–33], using the same discretization adopted here.

To obtain LCPs corresponding to different values of the pion mass at fixed physical strange quark mass, we assumed that there is a window within which the light quark mass m_l can be varied, at fixed β and m_s, without having a significant impact on the value of the lattice spacing. Although it is well known from arguments based on the hopping-parameter expansion that the effective β changes as we approach the quenched limit, our assumption is not unreasonable provided that we do not go too far from the physical point. Thus, we defined our LCPs with heavier-than-physical pions and physical strange quark as follows: after selecting a point $(\beta^{(\mathrm{phys})}, m_l^{(\mathrm{phys})}, m_s^{(\mathrm{phys})})$ along the physical LCP, we changed the bare light mass m_l keeping $\beta = \beta^{(\mathrm{phys})}$ and $m_s = m_s^{(\mathrm{phys})}$ fixed, where the superscript "(phys)" stands for bare parameters drawn from the physical LCP. We here note that the same procedure, with the same lattice discretization used here, was followed in Ref. [16] to take the chiral limit.

In order to verify that our assumptions are correct, we explicitly checked that the value of the lattice spacing did not change within our typical uncertainties. We fixed the scale by using the quantity w_0, based on the gradient flow [34]. Such quantity was assumed independent of the pion mass, and the same value was used to obtain a for all the ensembles considered in this work (cf. also Ref. [34] on this point). Using this prescription, we observe that the lattice spacing changes at most by $\sim 2\%$ among ensembles with different values of m_l, i.e., within the quoted uncertainties for a, thus confirming the validity of our procedure to fix the LCPs with unphysical pions.

We performed simulations for $m_l = 4, 6, 9\, m_l^{(\mathrm{phys})}$ with $\beta = \beta^{(\mathrm{phys})}$ and $m_s = m_s^{(\mathrm{phys})}$. Concerning simulations at the physical point, instead, we used some of the gauge ensembles that were previously generated for our paper [10]. Finally, concerning the lattice volume, the size of the box was always chosen in order to stay within the range $\ell \equiv aN_s = 2.7$ – 3.1 fm, corresponding to $M_\pi \ell \gtrsim 2$. As we will discuss in Sec. 2.2, this is largely sufficient to contain finite size effects affecting the computation of the chiral condensate. A full summary of our simulation parameters is shown in Tab. 1.

2.2 The Banks–Casher relation on the lattice

The properties of the low-lying spectrum of the massless Dirac operator $\displaystyle{\not{D}}$ encode information about the chiral condensate via the Banks–Casher relation [35]:

$$\lim_{\lambda \to 0} \lim_{m \to 0} \lim_{V \to \infty} \rho(\lambda, m) = \frac{\Sigma}{\pi}, \tag{2.4}$$

$R \equiv m_l/m_s$	$m_l/m_l^{(\text{phys})}$	β	N_s	am_l	am_s	a [fm]
1/28.15 $\simeq 0.0355$	1	3.750	24	0.0018	0.0503	0.1249
		3.850	32	0.0014	0.0394	0.0989
		3.938	32	0.0012	0.0330	0.0824
		4.020	40	0.0010	0.0281	0.0707
4/28.15 $\simeq 0.1421$	4	3.678	20	0.0088	0.0621	0.1515
		3.750	24	0.0072	0.0503	0.1265
		3.868	32	0.0054	0.0379	0.0964
		3.988	40	0.0042	0.0299	0.0758
6/28.15 $\simeq 0.2131$	6	3.678	20	0.0132	0.0621	0.1532
		3.750	24	0.0107	0.0503	0.1278
		3.868	32	0.0081	0.0379	0.0976
		3.988	40	0.0064	0.0299	0.0764
9/28.15 $\simeq 0.3197$	9	3.678	20	0.0199	0.0621	0.1556
		3.750	24	0.0161	0.0503	0.1297
		3.868	32	0.0121	0.0379	0.0989
		3.988	40	0.0095	0.0299	0.0768

Table 1: *Summary of simulation parameters used in this work. The bare parameters and lattice spacings of the points with $m_l = m_l^{(\text{phys})}$ have been fixed according to the LCP determined in Refs. [31–33], with $M_\pi = M_\pi^{(\text{phys})} = 135$ MeV and $R = m_l/m_s = R^{(\text{phys})} = 1/28.15$. Concerning points with $m_l/m_l^{(\text{phys})} \neq 1$, the lattice spacings have been determined with the w_0 scale setting approach [34] with $a \sim 2\%$ error, and their value in fm units was obtained assuming $w_0 = 0.1757(12)$ fm [34] for all ensembles, independently of the pion mass.*

where $\rho(\lambda, m)$ is the spectral density of the eigenvalues $i\lambda$ of $\not{D}$,

$$\rho(\lambda, m) = \frac{1}{V} \sum_k \langle \delta(\lambda - \lambda_k) \rangle. \tag{2.5}$$

On the lattice, in order to extract the chiral condensate from the low-lying spectrum of the lattice Dirac operator, a more convenient quantity to work with is the *mode number* [26]:

$$\langle \nu(M) \rangle = V \int_{-M}^{M} \rho(\lambda, m) d\lambda, \tag{2.6}$$

where V is the $4d$ space-time volume, and $\langle \nu(M) \rangle$ stands for the mean number of eigenmodes of $\not{D}$ whose absolute value lies below the threshold M. This quantity contains the same physical information with respect to the spectral density; as a matter of fact, in the chiral limit and sufficiently close to the origin, we expect from the Banks–Casher relation:

$$\langle \nu(M) \rangle = \frac{2}{\pi} V \Sigma M, \tag{2.7}$$

plus higher-order terms in M. The method proposed by Giusti and Lüscher [26] to extract the chiral condensate is based on Eq. (2.7): it consists in computing numerically the mode

number, then performing a linear fit of $\langle\nu\rangle$ as a function of M in a region close enough to the origin. The slope of such linear fit is the condensate, modulo overall factors.

The mode number can be determined quite accurately on the lattice, either by means of noisy estimators (as done in Ref. [26]) or by directly computing the first lowest eigenvalues of the discretized Dirac operator, which is the strategy followed in this paper. In the case of the massless staggered Dirac operator D_{stag}, the spectrum is made of purely imaginary numbers, which appear in complex conjugate pairs. Therefore, we solved the following eigenproblem numerically, using the `ARPACK` libraries and computing the first few hundred eigenvalues and eigenvectors:

$$iD_{\text{stag}}u_\lambda = \lambda u_\lambda, \qquad \lambda \in \mathbb{R}, \tag{2.8}$$

where D_{stag} is the very same operator used for sea quarks. Then, we simply computed:

$$\langle\nu_{\text{stag}}(M)\rangle = 2\langle\#\lambda \text{ with } 0 < \lambda < M\rangle, \tag{2.9}$$

where ν_{stag} stands for the number of staggered modes falling below M. Since the spectrum of D_{stag} becomes four-fold degenerate in the continuum limit, due to the taste degeneracy, in the continuum limit we expect the counting of staggered modes to become equal to n_t times the counting of modes of the Dirac operator for a single flavor, where $n_t = 2^{d/2} = 4$ denotes the number of different staggered tastes. Therefore, in order to recover the proper continuum limit for the mode number, and thus for the chiral condensate, we have to take into account such mode over-counting as follows:

$$\langle\nu_{\text{stag}}(M)\rangle = n_t\langle\nu(M)\rangle. \tag{2.10}$$

Thus, Eq. (2.7) with staggered quarks is modified as follows:

$$\langle\nu_{\text{stag}}(M)\rangle = n_t\frac{2}{\pi}V\Sigma M. \tag{2.11}$$

Let us now discuss how we renormalize Eq. (2.11) in our setup. The spectral threshold M renormalizes as a quark mass [26, 36], which in a staggered discretization renormalizes only multiplicatively. Therefore, the ratio of M to any quark mass is a Renormalization Group (RG) invariant quantity. Since in our setup the strange mass is always kept at the physical point and the light mass is varied, it is natural to use the former to renormalize M. Using the fact that the mode number is an automatically RG-invariant quantity [26], it is clear that it is sufficient to multiply and divide for m_s in Eq. (2.11) to obtain a fully renormalized relation that can be used in our numerical calculations:

$$\langle\nu_{\text{stag}}(M/m_s)\rangle = n_t\frac{2}{\pi}V(\Sigma m_s)\left(\frac{M}{m_s}\right). \tag{2.12}$$

Therefore, by performing a linear fit of the staggered mode number $\langle\nu_{\text{stag}}\rangle$ as a function of the RG-invariant ratio M/m_s, we can extract the RG-invariant quantity Σm_s according to Eq. (2.12).

As a final remark, we want to discuss finite-mass and finite volume effects. As for the former, we stress that the quantity extracted from the linear best fit of the mode number

can be interpreted as a physical quark condensate only in the chiral limit $m_l \to 0$. At finite light sea quark mass, the quantity we extract will be actually an "effective" mass-dependent condensate, needing extrapolation towards the chiral limit. The mass dependence of the effective condensate has been worked out in [26] using ChPT and, at LO in the quark mass, is expected to be linear in m_l.

Concerning finite volume effects, in Ref. [26] the authors have also worked out the approach to the thermodynamic limit of the effective condensate within ChPT, finding that finite volume corrections are not exponentially suppressed in $M_\pi \ell$ but in $M_0 \ell$, where the relevant scale is given by:

$$M_0^2 = \frac{2\Sigma M}{F_\pi^2} = M_\pi^2 \frac{1}{R} \frac{M}{m_s}, \tag{2.13}$$

with M the same scale appearing in Eq. (2.6) and $\ell \equiv aN_s$. As we will show in the following, the sizes of our lattices, which satisfy $M_\pi \ell \gtrsim 2$, and the value of M/m_s used in this work, are sufficient to contain finite size effects, as they correspond to $M_0 \ell \gtrsim 4$.

2.3 The quark mass dependence of the pion mass

There are different and complementary ways of computing the chiral condensate from the lattice other than the mode number. The most straightforward one relies on the GMOR relation in Eq. (1.3), which in the case of 2 degenerate light flavors becomes:

$$M_\pi^2 = \frac{2\Sigma}{F_\pi^2} m_l. \tag{2.14}$$

From the point of view of lattice calculations, numerical determinations of the pion mass can be fitted to Eq. (2.14) as a function of m_l to extract the ratio of LECs Σ/F_π^2, from which we can extract Σ once F_π has been taken out.

Both the pion mass and the pion decay constant can be extracted from the correlator of the appropriate lattice staggered interpolating operator of the physical pion $P(t) = \sum_{\vec{x}} P(t, \vec{x})$ [37]. As a matter of fact, for sufficiently large time separations, the correlator is expected to be described by a single exponential of the type:

$$C_\pi(t) = \langle P(t)P(0) \rangle \underset{t\to\infty}{\sim} A_\pi \left[e^{-M_\pi t} + e^{-M_\pi(\ell - t)} \right], \tag{2.15}$$

where M_π is the pion mass, and where the pre-factor A_π is the matrix element

$$A_\pi = |\langle \Omega | \overline{u}\gamma_5 d | \pi(\vec{p} = \vec{0}) \rangle|^2 / M_\pi. \tag{2.16}$$

Recalling the definition of F_π in Eq. (1.2) and using the PCAC relation, one quickly arrives to the following relation [16]:

$$F_\pi = m_l \sqrt{\frac{A_\pi}{M_\pi^3}} = m_s R \sqrt{\frac{A_\pi}{M_\pi^3}}. \tag{2.17}$$

2.4 The quark mass dependence of the topological susceptibility

Another strategy to obtain the chiral condensate is to study the behavior of the topological susceptibility (here $G_{\mu\nu}$ denotes the gauge field strength tensor)

$$\chi = \frac{\langle Q^2 \rangle}{V}, \qquad Q = \frac{1}{32\pi^2}\varepsilon_{\mu\nu\rho\sigma}\int \mathrm{Tr}\left\{G_{\mu\nu}(x)G_{\rho\sigma}(x)\right\}d^4x, \qquad (2.18)$$

as a function of the light quark mass. As a matter of fact, ChPT with 2 degenerate light flavors predicts at LO:

$$\chi = \frac{1}{2}\Sigma m_l, \qquad (2.19)$$

where the vanishing of χ in the chiral limit is a well known hallmark of the Index theorem. Thus, the chiral condensate can also be inferred from the slope of the topological susceptibility as a function of m_l (see, e.g., Ref. [8], where such strategy was used adopting Twisted Mass Wilson fermions).

Several equivalent definitions of the topological charge can be taken on the lattice, differing among themselves for lattice artifacts, but all agreeing in the continuum limit. They can be broadly divided into gluonic definitions, based on straightforward discretizations of $G\widetilde{G}$ computed on smoothened configurations [38–50], and fermionic definitions, based instead on the Index theorem.

As it has been extensively reported in the recent literature, gluonic definitions of the topological susceptibility are typically affected by large corrections to the continuum limit, which can be essentially traced back to the absence of exact zero-modes in the lattice Dirac operator, which is not able to properly suppress configurations with non-zero topological charge [4–10]. On the other hand, definitions based on spectral projectors of the lowest-lying modes of the discretized Dirac operator have been shown numerically to suffer for much smaller lattice artifacts, allowing to control systematical errors on the continuum extrapolation more easily [8, 10, 26, 27, 51].

In this work we will consider a fermionic definition of the topological charge, based on spectral projectors [8, 26, 27, 51] on the lowest-lying modes of the staggered operator. Such definition, worked out and probed in the quenched case in Ref. [36], has been applied both at zero and at finite temperature in Ref. [10], where it has been shown to yield agreeing results with the standard gluonic definition in the continuum limit, but suffering for much smaller lattice artifacts.

The idea is to define a lattice topological charge as

$$Q_{\mathrm{SP}}^{(0)} = \frac{1}{n_t}\sum_{|\lambda|\leq M} r_\lambda, \qquad r_\lambda = u_\lambda^\dagger \Gamma_5 u_\lambda, \qquad (2.20)$$

with Γ_5 the staggered definition of γ_5. Here, the pseudo-chiralities r_λ, defined from the very same eigenvectors u_λ of the eigenproblem in Eq. (2.8), are real numbers with absolute value between 0 and 1. In the continuum limit, instead, we expect $r_{\lambda=0} = \pm 1$ and $r_{\lambda\neq 0} = 0$, thus Eq. (2.20) will simply reduce to the Index theorem for any value of M, which at this level is a free parameter that can be thought of as an intrinsic UV cut-off of the spectral

definition, similar to the UV cut-off introduced by smoothing when considering gluonic definitions. Note again the presence of a factor of $1/n_t$ to take into account the mode over-counting due to taste degeneration.

This definition of the lattice charge can be proven to renormalize only multiplicatively [26, 36]:

$$Q_{\mathrm{SP}} = Z_{\mathrm{SP}}Q_{\mathrm{SP}}^{(0)}, \tag{2.21}$$

$$Z_{\mathrm{SP}} = \sqrt{\frac{\langle \mathrm{Tr}\,\{\mathbb{P}_M\}\rangle}{\langle \mathrm{Tr}\,\{\Gamma_5\mathbb{P}_M\Gamma_5\mathbb{P}_M\}\rangle}}\ , \tag{2.22}$$

where we have introduced the spectral projector

$$\mathbb{P}_M \equiv \sum_{|\lambda|\leq M} u_\lambda u_\lambda^\dagger\ . \tag{2.23}$$

Using Eq. (2.23), the definition in Eq. (2.20) can be rewritten as:

$$Q_{\mathrm{SP}}^{(0)} = \mathrm{Tr}\,\{\Gamma_5\mathbb{P}_M\}\ . \tag{2.24}$$

The traces appearing in Eq. (2.22) can be easily computed from the eigenvalues and eigenvectors of D_{stag}. As a matter of fact, $\langle \mathrm{Tr}\,\{\mathbb{P}_M\}\rangle$ is simply the mode number $\langle \nu_{\mathrm{stag}}(M)\rangle$; the denominator, instead, can be computed from the following spectral sum:

$$\langle \mathrm{Tr}\,\{\Gamma_5\mathbb{P}_M\Gamma_5\mathbb{P}_M\}\rangle = \sum_{|\lambda|\leq M}\sum_{|\lambda'|\leq M} |u_{\lambda'}^\dagger\Gamma_5 u_\lambda|^2. \tag{2.25}$$

The final spectral expression of the topological susceptibility can then be written as:

$$\chi_{\mathrm{SP}} = \frac{\langle Q_{\mathrm{SP}}^2\rangle}{V} = \frac{1}{n_t^2}\frac{\langle \mathrm{Tr}\{\mathbb{P}_M\}\rangle}{\langle \mathrm{Tr}\{\Gamma_5\mathbb{P}_M\Gamma_5\mathbb{P}_M\}\rangle}\frac{\langle \mathrm{Tr}\{\Gamma_5\mathbb{P}_M\}^2\rangle}{V}\ . \tag{2.26}$$

As a final remark, we briefly discuss the role of M. As we have already stressed, continuum results should not depend on M, as in that limit only zero-modes will contribute to the topological charge. Thus, we only expect lattice artifacts to depend on the choice of this threshold. In Refs. [8, 10] it was actually shown that this is the case, and that with a suitable choice of M it is possible to reduce dramatically lattice artifacts affecting the gluonic definition of the topological susceptibility. Following the lines of Ref. [10], we will thus compute the continuum limit of χ_{SP} for several values of M, in order to ensure that the choice of this quantity does not introduce any source of systematical errors.

3 Numerical results

In this section we will present our numerical results for the chiral condensate. We will present three different calculations, relying respectively on the mode number, the pion mass and the topological susceptibility. In all cases, we will perform controlled continuum at fixed pion mass, followed by a controlled chiral extrapolation. Finally, we will also perform a global fit of our data imposing that they are all described by the same value of the condensate.

3.1 Chiral condensate from the mode number

In this section we will discuss our determination of the chiral condensate from the mode number. First of all, in order to determine a reasonable fit range for the mode number where higher-order corrections in M are negligibile, we have looked for a common plateau region for the spectral densities determined for the finest lattice spacings at the various quark masses. Such determinations are shown in Fig. 1. From our results it is clear that in the range $\lambda/m_s \in [0.075, 0.15]$ the spectral density is fairly constant for all ensembles, thus it is reasonable to assume that higher-order terms in λ can be neglected in this interval. Therefore, we will use this range for the linear best fit of the mode number using the Giusti–Lüscher method.
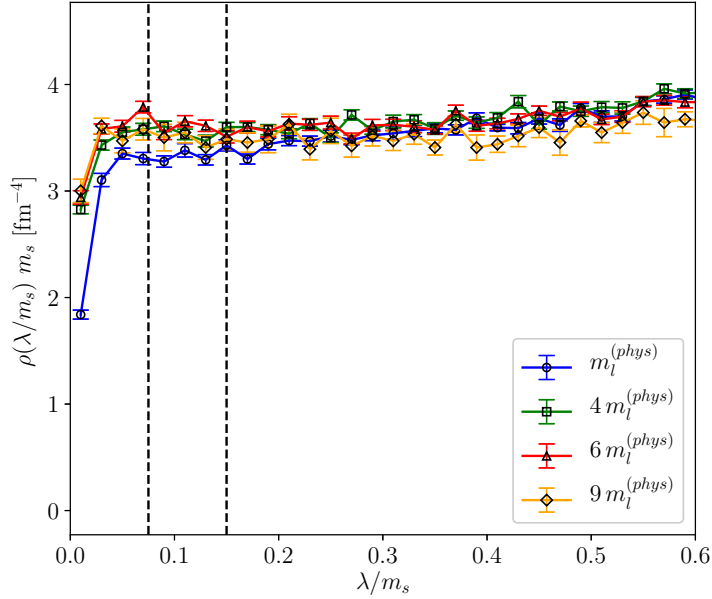
Figure 1: *Behavior of the RG-invariant spectral density $m_s\rho(\lambda/m_s)$ as a function of the RG-invariant ratio λ/m_s for the lattices with the finest lattice spacing, and for all explored values of m_l. The range between the two dashed vertical lines, $\lambda/m_s \in [0.075, 0.15]$, is the one chosen to perform the linear best fit of the mode number.*

Within the range earlier determined, we observe from Fig. 2 that, as expected, the mode number can be reliably described by a linear rise in M/m_s. Performing the following best fit, where s denotes the slope of the mode number in the middle point of the fit range,

$$\langle\nu_{\text{stag}}(M/m_s)\rangle = s\frac{M}{m_s}, \tag{3.1}$$

we obtain the effective chiral condensate as:

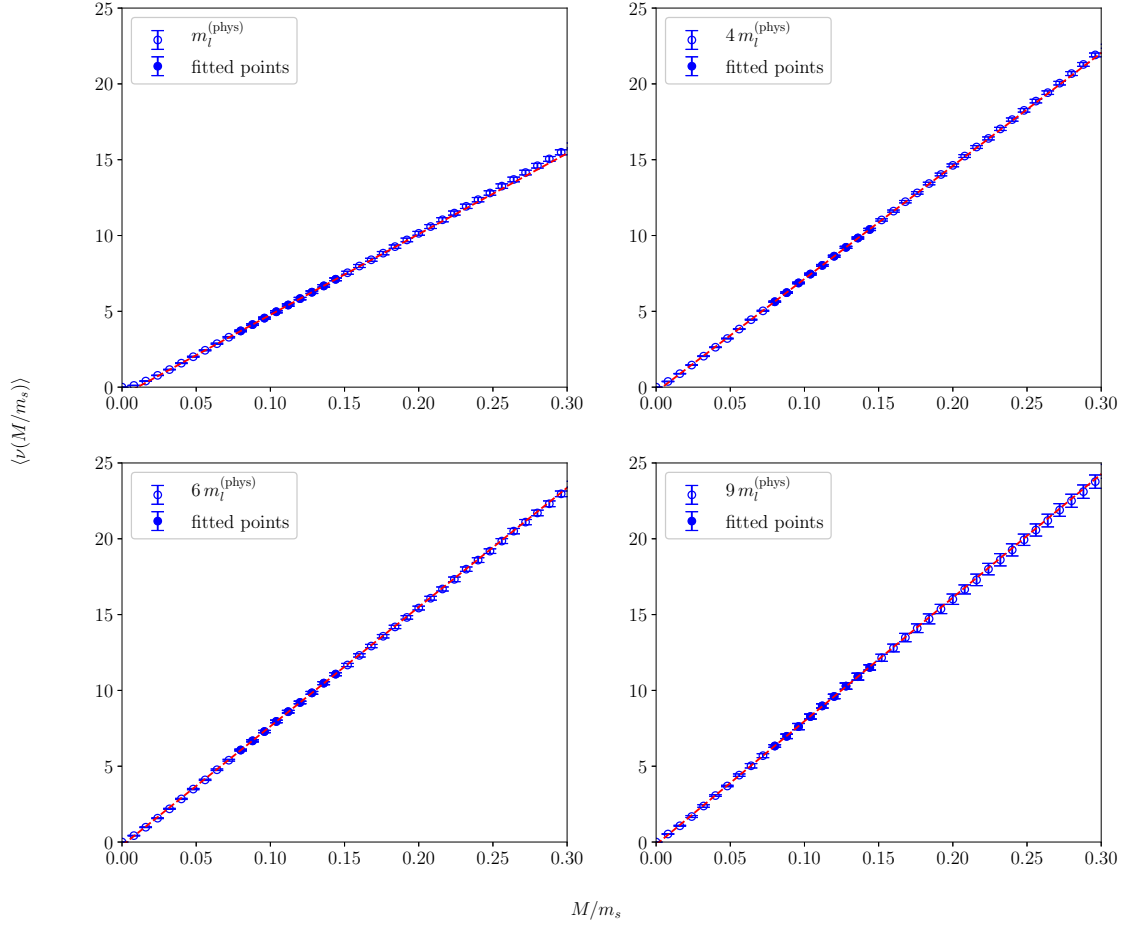$$\Sigma m_s = \frac{\pi}{2}\frac{s}{n_t V}, \qquad V = (aN_s)^4. \tag{3.2}$$

Figure 2: *Linear best fit of the physical mode number $\langle \nu \rangle = \langle \nu_{\text{stag}} \rangle / 4$ as a function of M/m_s for the finest lattice spacing for each value of m_l. Filled points in the range $M/m_s \in [0.075, 0.15]$ are those included in the best fits, depicted as dashed lines.*

In order to take out the strange quark mass in the latter expression for $\Sigma m_s = \Sigma_{\text{R}} m_s^{(\text{R})}$, we use the following value for the renormalized mass:

$$m_s^{(\text{R})} = 92.4(1.5) \text{ MeV}. \tag{3.3}$$

This value was obtained in the $\overline{\text{MS}}$ renormalization scheme at the conventional renormalization point $\mu = 2$ GeV from a $2+1$ lattice QCD calculation involving staggered fermions in Ref. [52]. After removing the factor of $m_s^{(\text{R})}$ via the renormalized mass above, we are thus left with the renormalized chiral condensate Σ_{R}, which of course has to be understood as expressed in the $\overline{\text{MS}}$ scheme at $\mu = 2$ GeV as well. Our determinations of Σ_{R} as a function of the lattice spacing a and of the light quark mass m_l are collected in Tab. 2.

$R \equiv m_l/m_s$	$m_l/m_l^{\text{(phys)}}$	a [fm]	$\Sigma_{\text{R}}^{1/3}$ [MeV]
1/28.15 $\simeq 0.0355$	1	0.1249	282.0(1.6)
		0.0989	282.1(1.6)
		0.0824	282.8(1.7)
		0.0707	277.9(1.6)
		0	275.0(5.0)
4/28.15 $\simeq 0.1421$	4	0.1515	284.3(1.5)
		0.1265	283.0(1.5)
		0.0964	283.3(1.5)
		0.0758	283.7(1.6)
		0	284.0(2.5)
6/28.15 $\simeq 0.2131$	6	0.1532	283.2(1.5)
		0.1278	282.2(1.5)
		0.0976	283.3(1.6)
		0.0764	285.5(1.6)
		0	287.0(2.5)
9/28.15 $\simeq 0.3197$	9	0.1556	282.6(1.5)
		0.1297	281.0(1.5)
		0.0989	283.4(1.6)
		0.0768	286.8(1.9)
		0	289.0(5.0)

Table 2: *Values of the cubic root of the effective chiral condensate obtained from the mode number for each value of m_l and for each lattice spacing. The values of $\Sigma_{\text{R}}^{1/3}$ at $a = 0$ correspond to the extrapolations towards the continuum limit.*

Before proceeding to discuss the continuum and chiral limits, let us make a remark about finite size effects. First of all, plugging $M_\pi = 135$ MeV, $M/m_s = 0.15$ and $1/R = 28.15$ in Eq. (2.13), we obtain that the mass scale controlling finite size effects affecting Σ computed from the mode number is $M_0 \simeq 2M_\pi$. Since we use lattices with $M_\pi \ell \gtrsim 2$, we have $M_0 \ell \gtrsim 4$, which is largely sufficient to maintain the magnitude of finite volume corrections below our typical statistical error, of the order of a few percent. This estimation is also in agreement with the prescription given in [26], where the authors estimate that lattices with $\ell \gtrsim 2$ fm ($M_\pi \ell \gtrsim 1.4$) are sufficient to keep finite volume effects below the percent level. In any case, for a particular point of our ensembles we also considered two additional lattice volumes in order to directly check the absence of any dependence on the box size for the volumes adopted in this work, cf. Fig. 3.

As it can be appreciated, varying the lattice size from $M_0 \ell \simeq 3$ to $M_0 \ell \simeq 5$ only yields a significant difference for the spectral density in the two smallest bins, which are those that are expected to suffer more from Finite Size Effects (FSEs), cf. Fig. 3 on the top. Above $M/m_s = 0.05$, instead, we observe no significant difference in the spectral densities.
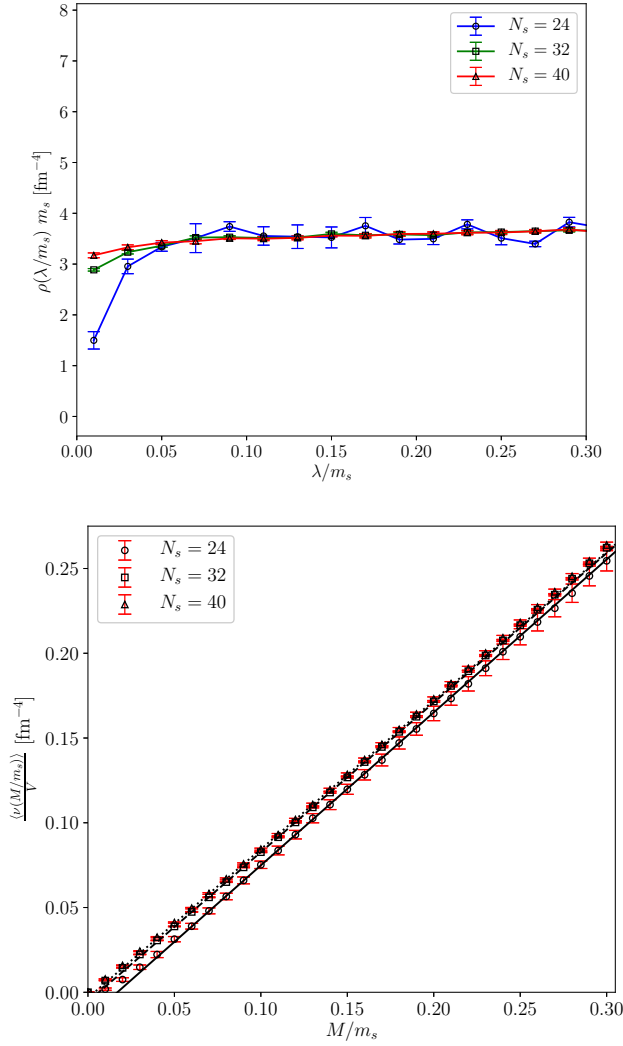
Figure 3: *Comparison of the spectral densities $m_s\rho(\lambda/m_s)$ (top panel) and of the mode number densities $\langle\nu(M/m_s)\rangle/V$ [fm^{-4}] (bottom panel) for 3 different lattices with sizes $N_s = 24, 32, 40$, corresponding to $M_0\ell \simeq 3, 4, 5$, for our point with $a = 0.0964$ fm, $\beta = 3.868$ and $m_l = 4m_l^{\rm (phys)}$.*

Since we are fitting the mode number in $[0.075, 0.150]$, we thus expect no FSEs in the slopes of the mode numbers. As a matter of fact, the mode numbers for these 3 lattices have parallel slopes, and $\langle\nu\rangle$ for $M_0\ell \simeq 3$ only differs from the ones obtained at $M_0\ell \simeq 4$ and $M_0\ell \simeq 5$ for an overall shift (due to the FSEs affecting the lowest modes), cf. Fig. 3 on the bottom. In the end, we obtain $\Sigma_{\rm R}^{1/3} = 285(2), 283(2), 283(2)$ MeV, for, respectively, $M_0\ell = 3, 4, 5$. Thus, we conclude that our determinations of the condensate from the mode number obtained on lattices with $M_0\ell \simeq 4$ or larger are not affected by significant FSEs at the current level of precision.

Once determinations of the effective chiral condensate have been obtained as a function of the lattice spacing a and of the light quark mass m_l, we first take the continuum limit

at fixed m_l, i.e., at fixed value of $R = m_l/m_s$, assuming standard $O(a^2)$ corrections:

$$\Sigma_{\mathrm{R}}^{1/3}(a, R) = \Sigma_{\mathrm{R}}^{1/3}(R) + c_1(R)\, a^2 + o(a^2). \tag{3.4}$$

Continuum extrapolations are shown in Fig. 4. As it can be observed, data for the three finest lattice spacings are perfectly described by linear corrections in a^2. A parabolic best fit of our data including also the coarsest lattice spacing gives agreeing results within the errors. Therefore, we take the result of the linear fit with 3 points as our estimate of the continuum limit, which is reported in Tab. 2 as the determination for $a = 0$.
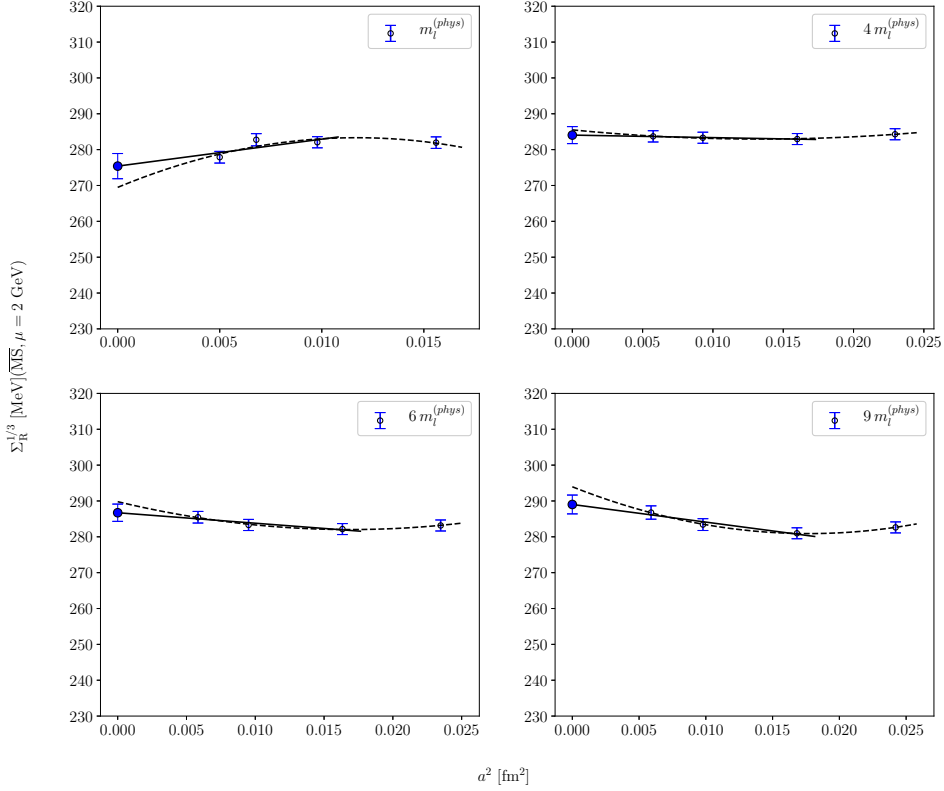
Figure 4: *Continuum limit extrapolation of $\Sigma_{\mathrm{R}}^{1/3}$ for each value of m_l obtained from the mode number. Solid lines represent linear fits in a^2 to the 3 finest lattice spacings, with the filled point in $a = 0$ representing the corresponding continuum limits. Dashed lines represent instead parabolic fits in a^2 to all of our data, including also the determinations at the coarsest lattice spacing.*

Finally, we extrapolate our continuum results towards the chiral limit according to the following fit function [26]:

$$\Sigma_{\rm R}^{1/3}(R) = \Sigma_{\rm R}^{1/3} + c_2\,R + o(R), \tag{3.5}$$

where eventually $\Sigma_{\rm R}$ represents our final result for the condensate. The chiral extrapolation is shown in Fig. 5. As it can be appreciated, our data are perfectly described by a linear function in $R = m_l/m_s$ for all explored values of the light quark mass, as expected from chiral perturbation theory. By fitting all available points, we find $\Sigma_{\rm R}^{1/3} = 276(4)$ MeV. A linear fit to the points corresponding to the three lightest masses gives the perfectly compatible result $\Sigma_{\rm R}^{1/3} = 274(5)$ MeV. In the end, from the mode number we quote the following final result:

$$\Sigma_{\rm R}^{1/3} = 276(4) \text{ MeV} \qquad \text{(mode number)}. \tag{3.6}$$

Before commenting this number further, we will first proceed with the computation of the chiral condensate with different methods involving different observables, in order to check the consistency of our approach.
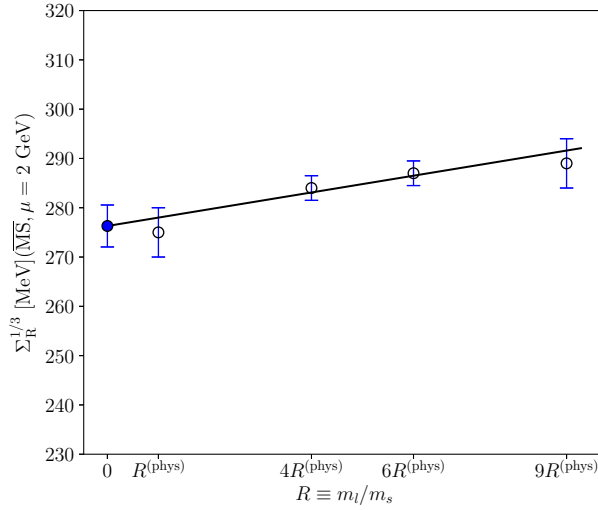
Figure 5: *Chiral limit extrapolation of $\Sigma_{\rm R}^{1/3}$ at fixed m_s as a function of $R = m_l/m_s$. The solid line represents the result of the best fit performed according to Eq. (3.5) and including all available values of R. The filled point at $R = 0$ represents the final value for the chiral condensate extracted from the mode number.*

3.2 Chiral condensate from the pion mass

In this section we will extract the chiral condensate from the quark mass dependence of the pion mass. From pion correlators, it is possible to extract both the pion mass M_π and the pion decay constant F_π. We will need both quantities to extract the chiral condensate,
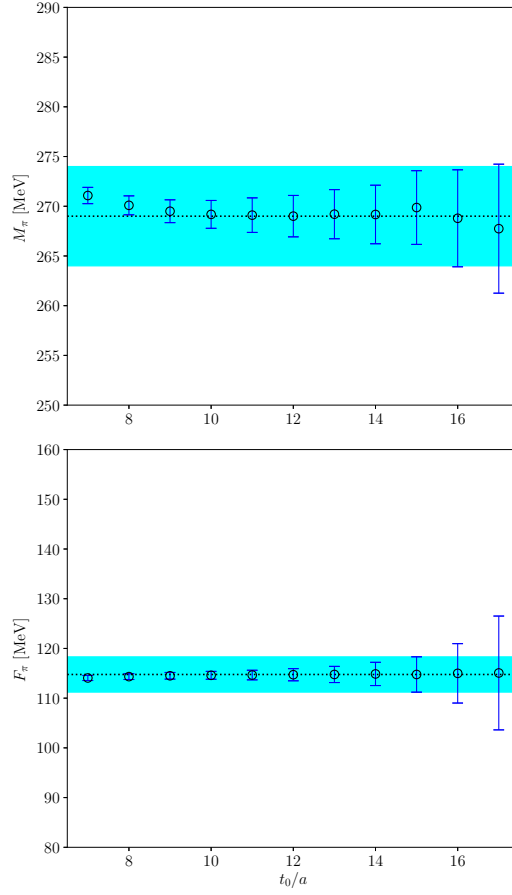
Figure 6: *Pion mass M_π and pion decay constant F_π as a function of the lower bound of the fit range t_0 (expressed in lattice units). Shaded areas represent our final result for both quantities.*

as, cf. Eq. (2.14):

$$M_\pi^2 = 2\frac{\Sigma}{F_\pi^2}m_l = 2\left(\frac{\Sigma m_s}{F_\pi^2}\right)R. \tag{3.7}$$

First of all, let us show an example of computation of M_π and F_π. We fitted our pion correlator $C_\pi(t)$ in the range $t/a \in [t_0/a; N_s - t_0/a]$ to the functional form reported in Eq. (2.15) for several values of t_0, looking for a pleateau in both quantities, in order to provide a robust estimation of both. The pion decay constant was obtained from Eq. (2.17) and using the value of $m_s^{(\mathrm{R})}$ in Eq. (3.3). An example of computation of the pion mass and decay constant is shown in Fig. 6.

Let us start our discussion from the pion decay constant. In Fig. 7 we show the extrapolation towards the continuum limit of $F_\pi(a, R)$ at fixed value of R assuming $O(a^2)$ corrections:

$$F_\pi(a, R) = F_\pi(R) + b_1(R)\,a^2 + o(a^2). \tag{3.8}$$

As it can be appreciated, our data can be reliably fitted by such functional form, and including/excluding the point relative to the coarsest lattice spacing has a minimal impact on the fit result. Thus, we take the result of the fit performed in the whole lattice spacing range as our continuum limit. All our determinations are reported in Tab. 3.
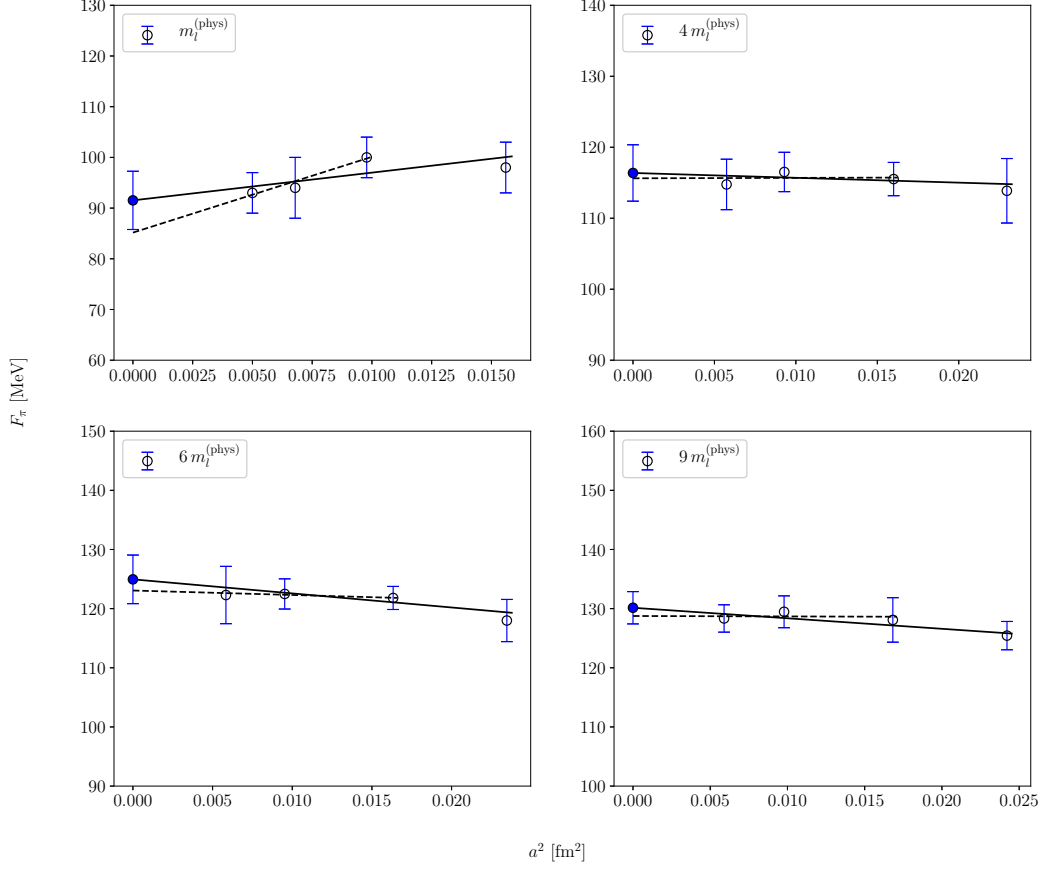
Figure 7: *Continuum limit extrapolation of $F_\pi(a, R)$ for all the lines of constant physics considered here. Solid and dashed lines represent, respectively, continuum extrapolations assuming $O(a^2)$ corrections to the points corresponding to the three finest lattice spacings and to all available points.*

Finally, we extrapolate our continuum results for F_π towards the chiral limit, using the following fit function modeled on ChPT [16]:

$$F_\pi(R) = F_\pi + b_2\, R. \tag{3.9}$$

In this case we observe that, although a linear fit in R can be performed in the whole available range, the slope changes visibly if the point relative to $R = 9R^{(\mathrm{phys})}$ is excluded from the fit, cf. Fig. 8. Thus, as our final result, we take the chiral limit obtained from the results of our 3 lightest LCPs:

$$F_\pi = 87.6(6.5) \text{ MeV}. \tag{3.10}$$

We now move to our results for M_π. Pion masses as a function of the lattice spacing are shown in Fig. 9. As expected, they are fairly constant as a function of a for each LCP. The shaded areas in the figure represent our final results for M_π for each value of R. All our determinations of M_π are collected in Tab. 4.

As it can be appreciated from Fig. 10, our results for M_π^2 can be nicely fitted with a linear function in R. First, we perform a linear fit where the chiral limit of the pion

$R \equiv m_l/m_s$	$m_l/m_l^{(\text{phys})}$	a [fm]	F_π [MeV]
1/28.15 $\simeq 0.0355$	1	0.1249	98(5)
		0.0989	100(4)
		0.0824	94(6)
		0.0707	93(4)
		0	92(6)
4/28.15 $\simeq 0.1421$	4	0.1515	114(5)
		0.1265	116(2)
		0.0964	117(3)
		0.0758	115(4)
		0	116(4)
6/28.15 $\simeq 0.2131$	6	0.1532	118(4)
		0.1278	122(2)
		0.0976	123(3)
		0.0764	122(5)
		0	123(5)
9/28.15 $\simeq 0.3197$	9	0.1556	125(2)
		0.1297	128(4)
		0.0989	129(3)
		0.0768	128(2)
		0	129(4)

Table 3: *Values of the pion decay constant as a function of the lattice spacing a and of the light quark mass m_l. The values of F_π at $a = 0$ correspond to the extrapolations towards the continuum limit.*
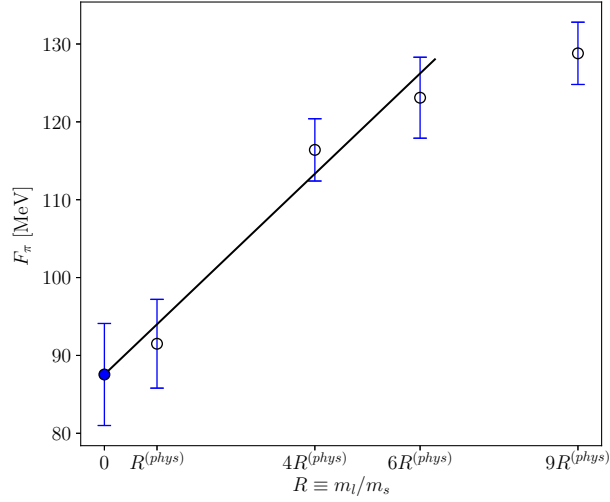
Figure 8: *Extrapolation towards the chiral limit of $F_\pi(R)$ as a function of R. The solid line represents a linear best fit in R excluding the point for $R = 9R^{(\text{phys})}$.*
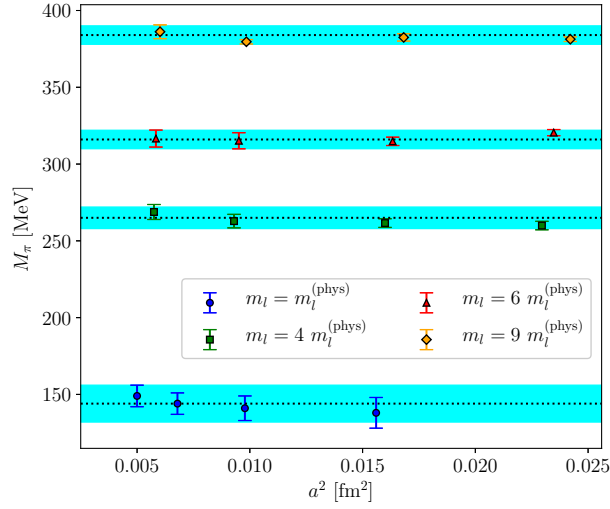
Figure 9: *Obtained results for the pion mass M_π as a function of the lattice spacing for each LCP. The shaded areas represent our final estimations of the pion masses for each LCP.*

mass is left as a free parameter. We find, using the number in Eq. (3.10) for the pion decay constant, $\Sigma_R^{1/3} = 264(14)$ MeV if all available points are included in the fit, and $\Sigma_R^{1/3} = 265(14)$ MeV if the heaviest pion is excluded. In both cases we find a vanishing chiral limit for M_π within errors. As a matter of fact, if we repeat this fit fixing the chiral limit of M_π to zero, we find $\Sigma_R^{1/3} = 270(14)$ MeV and $\Sigma_R^{1/3} = 271(14)$ MeV if the heaviest pion is included/excluded from the fit respectively. In the end, from the pion mass we quote the final result:

$$\Sigma_R^{1/3} = 267(15) \text{ MeV} \qquad \text{(pion mass)}. \qquad (3.11)$$
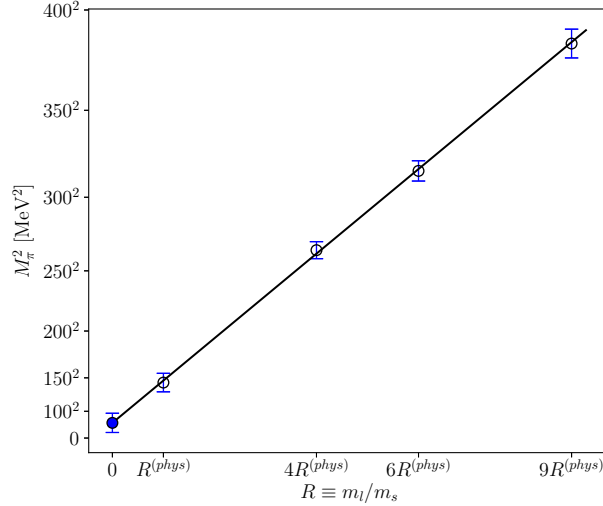
Figure 10: *Extrapolation towards the chiral limit of M_π^2 at fixed m_s as a function of $R = m_l/m_s$. The solid line is the result of a linear fit where the chiral limit of M_π^2 is left as a free parameter. We find such fit parameter to be compatible with zero within errors.*

$R \equiv m_l/m_s$	$m_l/m_l^{\text{(phys)}}$	a [fm]	$M_\pi(a)$ [MeV]	Final res. M_π [MeV]
$1/28.15$ $\simeq 0.0355$	1	0.1249	138(10)	144(12)
		0.0989	141(8)	
		0.0824	144(7)	
		0.0707	149(7)	
$4/28.15$ $\simeq 0.1421$	4	0.1515	260(3)	265(6)
		0.1265	262(3)	
		0.0964	263(4)	
		0.0758	269(5)	
$6/28.15$ $\simeq 0.2131$	6	0.1532	320(2)	316(6)
		0.1278	315(3)	
		0.0976	315(5)	
		0.0764	317(6)	
$9/28.15$ $\simeq 0.3197$	9	0.1556	381(1)	384(7)
		0.1297	382(2)	
		0.0989	380(1)	
		0.0768	386(4)	

Table 4: *Values of the pion mass M_π for each value of m_l and for each lattice spacing a.*

3.3   Chiral condensate from the topological susceptibility

In this section we will address the computation of the chiral condensate from the quark mass dependence of the topological susceptibility, according to the ChPT prediction in Eq. (2.19):

$$\chi = \frac{1}{2}\Sigma m_l = \frac{1}{2}(\Sigma m_s)R. \tag{3.12}$$

To keep the discussion more compact, here we will just show the computation of the continuum limit of χ for one line of constant physics, namely the one corresponding to $m_l = 4m_l^{\text{(phys)}}$. Concerning the computation of χ at the physical point, it has been already extensively discussed on the dedicated paper [10], thus, here we just take the result reported there. Finally, the results for the other two lines of constant physics with heavier-than-physical pions can be found in App. A.

First of all, we extrapolate our results towards the continuum limit using the fermionic discretization discussed in Sec. 2.4, and assuming the following fit function:

$$\chi_{\text{SP}}^{1/4}(a, M/m_s) = \chi^{1/4} + c_{\text{SP}}(M/m_s)\,a^2 + o(a^2). \tag{3.13}$$

In Fig. 11 on the left, we show a few examples of continuum extrapolations for some values of M/m_s. As it can be observed, our spectral definition suffers for mild lattice artifacts, and our determinations for the 3 finest lattice spacings can be reliably fitted

with a linear function in a^2. We also tried to perform parabolic fits in a^2 including also the determinations at the coarsest lattice spacing, obtaining agreeing results within errors. Thus, systematical errors related to the continuum extrapolation can be controlled solidly, and we take for each value of M/m_s the linear extrapolations obtained with 3 fitted points as our estimations of the continuum limit of $\chi_{\mathrm{SP}}^{1/4}(M/m_s)$.

In Fig. 11 on the right we show instead how the continuum extrapolations of $\chi_{\mathrm{SP}}^{1/4}(M/m_s)$ behave as a function of M/m_s. On general theoretical grounds, we expect the continuum limit of $\chi_{\mathrm{SP}}(M/m_s)$ to be independent of M/m_s. As it can be observed, continuum extrapolations of $\chi_{\mathrm{SP}}^{1/4}(M/m_s)$ as a function of M/m_s are all compatible among each other, as expected. Nonetheless, we opt for a conservative error estimation and we also include any small variation observed as a function of M/m_s to our final error budget. Our final continuum results are reported in Tab. 12.
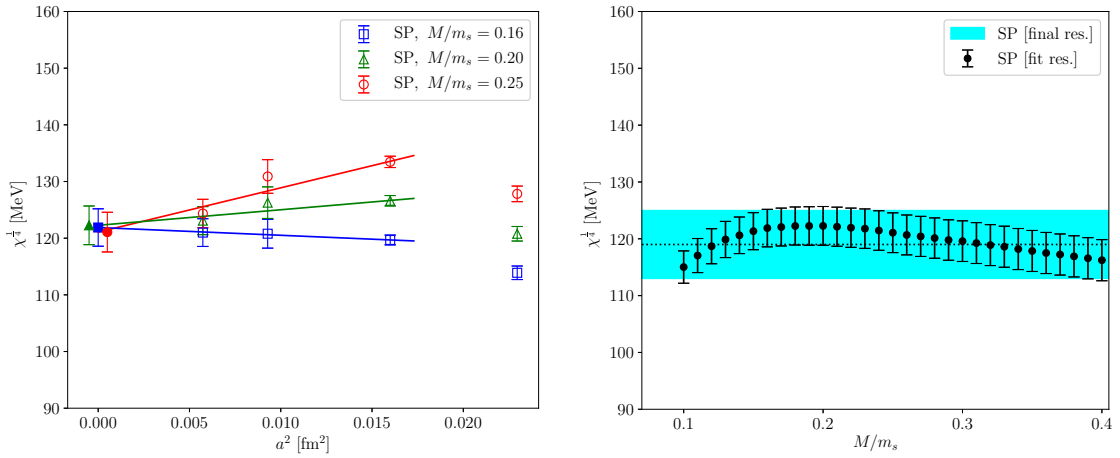
Figure 11: *Left panel: comparison of continuum limit extrapolations of $\chi_{\mathrm{SP}}^{1/4}(M/m_s)$ for $m_l = 4\,m_l^{(\mathrm{phys})}$ and for a few values of M/m_s. Straight lines refer to the continuum extrapolations obtained by fitting determinations obtained for the 3 finest lattice spacings with a linear function in a^2. Full points in $a = 0$ represent the corresponding continuum extrapolations. Right panel: continuum limits of $\chi_{\mathrm{SP}}^{1/4}$ obtained from spectral projectors at $m_l = 4\,m_l^{(\mathrm{phys})}$ for several values of M/m_s. The shaded area represents our final result for the continuum limit of χ_{SP}.*

$R \equiv m_l/m_s$	$m_l/m_l^{(\mathrm{phys})}$	$\chi^{1/4}$ [MeV]
$1/28.15 \simeq 0.0355$	1	80(10)
$4/28.15 \simeq 0.1421$	4	119(6)
$6/28.15 \simeq 0.2131$	6	125(5)
$9/28.15 \simeq 0.3197$	9	135(15)

Table 5: *Final continuum limit determinations of the fourth root of the topological susceptibility, obtained with the spectral projectors discretization. Errors on such determinations take into account all sources of systematic uncertainties (see the text for more details).*
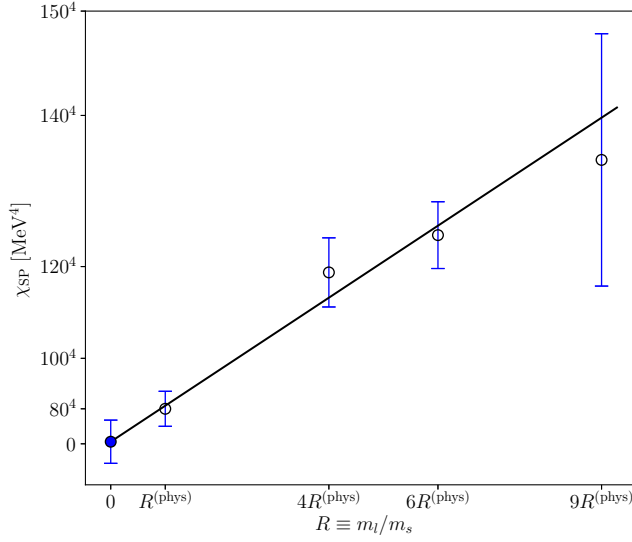
Figure 12: *Extrapolation towards the chiral limit of the continuum results for the topological susceptibility χ at fixed m_s as a function of $R = m_l/m_s$. The solid line is the result of a linear fit with the chiral limit left as a free parameter. We find such fit parameter to be compatible with zero within errors.*

As it can be appreciated from Fig. 12, our results for the topological susceptibility can be perfectly described by a linear function in R. First, we perform a linear fit where the chiral limit of χ is left as a free parameter. We find $\Sigma_R^{1/3} = 295(18)$ MeV if all available points are included in the fit, and $\Sigma_R^{1/3} = 297(19)$ MeV if the point with $R = 9R^{(\mathrm{phys})}$ is excluded. In both cases we find a vanishing chiral limit for χ within errors. As a matter of fact, if we repeat this fit fixing the chiral limit of χ to zero, we find $\Sigma_R^{1/3} = 297(12)$ MeV and $\Sigma_R^{1/3} = 298(12)$ MeV if the point at $9R^{(\mathrm{phys})}$ is included/excluded from the fit respectively. In the end, from the topological susceptibility we quote the final result:

$$\Sigma_R^{1/3} = 297(20) \text{ MeV} \qquad \text{(topological susceptibility)}. \tag{3.14}$$

3.4 Discussion of the obtained result and global fit

So far, we have obtained these three different determinations of the chiral condensate:

$$\Sigma_R^{1/3} = 276(4) \text{ MeV} \qquad \text{(from } \langle \nu \rangle \text{)}, \tag{3.15}$$

$$\Sigma_R^{1/3} = 267(15) \text{ MeV} \qquad \text{(from } M_\pi \text{)}, \tag{3.16}$$

$$\Sigma_R^{1/3} = 297(20) \text{ MeV} \qquad \text{(from } \chi \text{)}. \tag{3.17}$$

Since they all are in very good agreement among themselves, it is reasonable to perform a global fit of these quantities as a function of the ratio of quark masses R to provide a more stringent check of the consistency of these findings among themselves.

To this end, we perform a fit of the continuum limits of the effective condensate $\Sigma_R(R)$ extracted from the mode number, of $M_\pi^2(R)$ extracted from pion correlators and of the continuum limits of the spectral topological susceptibility $\chi(R)$, imposing a single fit parameter for the chiral condensate Σ_R, and using our result in Eq. (3.10) for the pion decay constant. Leaving the chiral limit of M_π and χ as free parameters, and including all available determinations in the best fit procedure, we find that our data can be perfectly
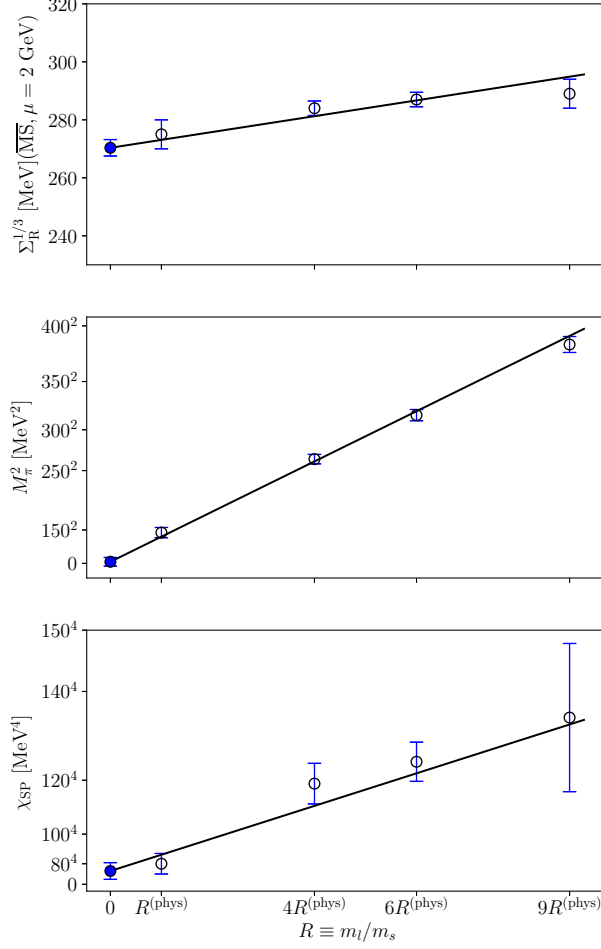
Figure 13: *Result of the global chiral fit to the continuum limits of the effective condensate obtained from the mode number (top plot), the continuum limits of M_π^2 (center plot) and the continuum limits of the topological susceptibility, obtained using the spectral projectors definition (bottom plot), imposing that all data sets are described by a single free fit parameter for the chiral condensate, and leaving the chiral limits of M_π and χ as free fit parameters.*

described by such global fit, just involving one free parameter for the chiral condensate. Such fit is shown in Fig. 13. It yields a reduced chi-squared $\tilde{\chi}/\text{dof} = 8.96/8$, vanishing chiral limits for M_π and χ within errors, and a value for the chiral condensate $\Sigma_R^{1/3} = 270(3)$ MeV. Excluding from the global fit our determinations obtained for the heaviest pion here considered, we find the perfectly agreeing result $\Sigma_R^{1/3} = 271(4)$ MeV. Also fixing the chiral limits of the pion mass and of the topological susceptibility to be zero does not change the obtained results, as we find: $\Sigma_R^{1/3} = 271(3)$ MeV and $\Sigma_R^{1/3} = 273(4)$ MeV if, respectively, quantities obtained for $R = 9R^{(\text{phys})}$ are included/excluded from the fit. Thus, in the end, we quote the following result for the chiral condensate from the global fit, which we also take as our final determination for Σ_R:

$$\Sigma_R^{1/3} = 270(3) \text{ MeV}, \qquad \text{(global fit)}. \tag{3.18}$$

Although the quantities involved in this fitting procedure have been computed on the same set of configurations, and are thus correlated, we expect such correlations to not have a significant impact, since the fitted observables are very different and affected by very different systematical errors, which have all been taken into account very conservatively. In any case, being the determination from the mode number much more precise than the others, we expect it to drive the result of the global fit. By looking at our final result in Eq. (3.18) we observe that this is the case, which makes us confident that the error estimate on our final result for the condensate is overall pretty solid.

As a final remark, let us comment that this result is in perfect agreement both with the phenomenological estimation given in the introduction, $\Sigma_{\text{pheno}}^{1/3} = 283(24)$ MeV, and with the world-average reported in the latest FLAG review for the SU(2) condensate obtained from $N_f = 2 + 1$ QCD: $\Sigma_{\text{FLAG}}^{1/3} = 272(5)$ MeV [25].

4 Conclusions

In this paper we have addressed the computation of the SU(2) chiral condensate from a staggered discretization of $2 + 1$ QCD.

Our calculation is based on 4 lattice spacing and 4 lines of constant physics with different values of the light quark mass, and the strange quark mass kept at the physical point. This allowed us to perform controlled continuum and chiral extrapolations.

Concerning the numerical strategies pursued in this work, our main approach relies on the extraction of the chiral condensate from the mode number using the Giusti–Lüscher method, based on the Banks–Casher relation. Such technique is implemented and applied to the staggered case for the first time in this paper.

Moreover, we checked carefully that perfectly agreeing results are obtained if the chiral condensate is extrated from the quark mass dependence of the pion mass or the quark mass dependence of the topological susceptibility, which we have computed from spectral projectors on the low-lying modes of the staggered operator. The agreement among such different determinations is further confirmed by a global fit of our data, assuming a single fit parameter for the chiral condensate, which provides an excellent description of our numerical results. Finally, as a by-product of our study, we are also able to provide an estimate of the pion decay constant in the chiral limit F_π.

In the end, we provide the following final results for the two SU(2) ChPT LECs:

$$\Sigma_{\text{R}}^{1/3} = 270(3) \text{ MeV}, \qquad (\overline{\text{MS}}, \, \mu = 2 \text{ GeV}), \tag{4.1}$$

$$F_\pi = 87.6(6.5) \text{ MeV}. \tag{4.2}$$

Our results are in excellent agreement both with the phenomenological estimation that can be obtained from the GMOR relation, $\Sigma_{\text{pheno}}^{1/3} = 283(24)$ MeV, and with the FLAG $2 + 1$ results: $\Sigma_{\text{FLAG}}^{1/3} = 272(5)$ MeV and $F_\pi|_{\text{FLAG}} = 86.6(6)$ MeV.

Acknowledgements

Appendix

A   Additional plots

In this appendix, we collect additional plots not shown in the main text. In Figs. 14, 15, 16 and 17 we show the linear fit to the mode number for all lattice spacings but the finest (which is reported in the main text), and for all LCPs. In Figs. 18 and 19 we show the extrapolation towards the continuum limit of the topological susceptibility for the LCPs corresponding to $m_l = 6, 9 \ m_l^{(\mathrm{phys})}$.
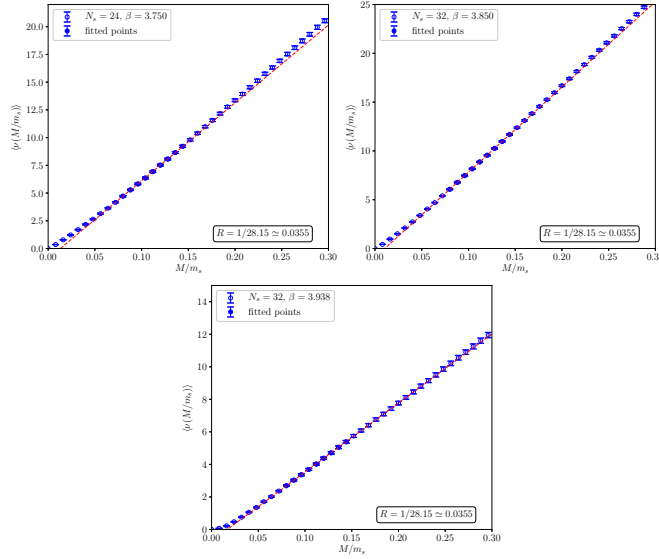

Figure 14: *Linear best fits of the physical mode number $\langle \nu \rangle = \langle \nu_{\mathrm{stag}} \rangle /4$ as a function of M/m_s for the 3 coarser lattice spacings at $m_l = m_l^{(\mathrm{phys})}$. Filled points in the range $M/m_s \in [0.075, 0.15]$ are those included in the best fits, depicted as dashed lines.*
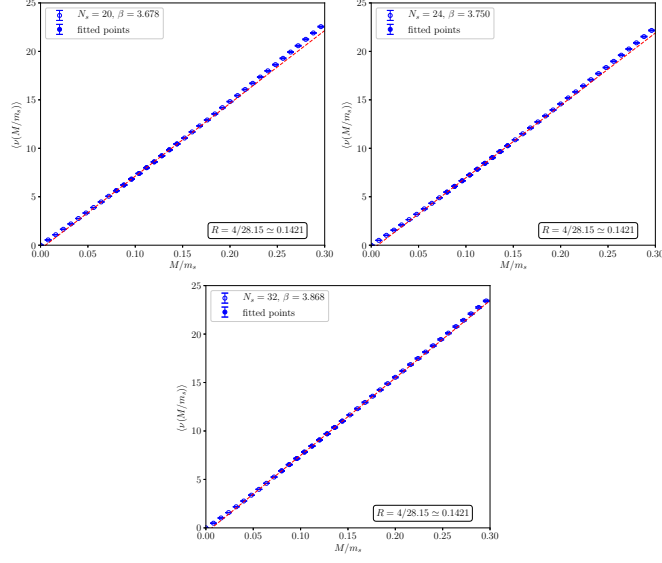
Figure 15: *Linear best fits of the physical mode number $\langle\nu\rangle = \langle\nu_{\mathrm{stag}}\rangle/4$ as a function of M/m_s for the 3 coarser lattice spacings at $m_l = 4\ m_l^{(\mathrm{phys})}$. Filled points in the range $M/m_s \in [0.075, 0.15]$ are those included in the best fits, depicted as dashed lines.*
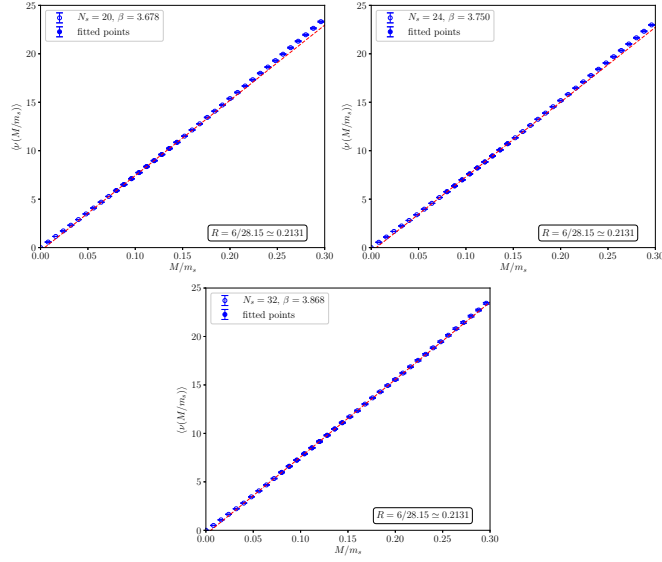

Figure 16: *Linear best fits of the physical mode number $\langle\nu\rangle = \langle\nu_{\mathrm{stag}}\rangle/4$ as a function of M/m_s for the 3 coarser lattice spacings at $m_l = 6\ m_l^{(\mathrm{phys})}$. Filled points in the range $M/m_s \in [0.075, 0.15]$ are those included in the best fits, depicted as dashed lines.*
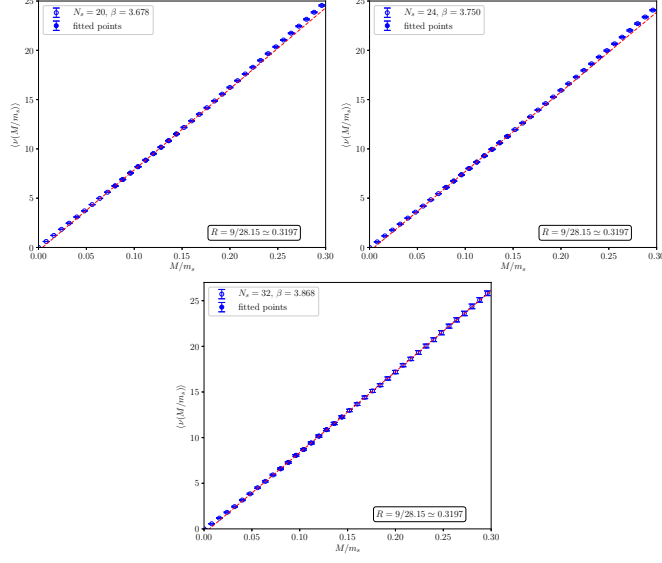
Figure 17: *Linear best fits of the physical mode number $\langle \nu \rangle = \langle \nu_{\mathrm{stag}} \rangle / 4$ as a function of M/m_s for the 3 coarser lattice spacings at $m_l = 9 \, m_l^{(\mathrm{phys})}$. Filled points in the range $M/m_s \in [0.075, 0.15]$ are those included in the best fits, depicted as dashed lines.*
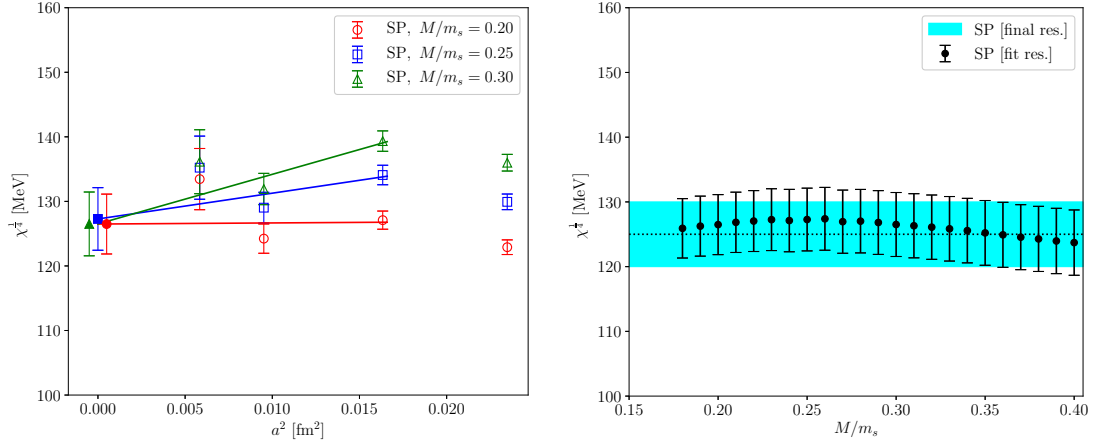

Figure 18: *Left panel: comparison of continuum limit extrapolations of $\chi_{\mathrm{SP}}^{1/4}(M/m_s)$ for $m_l = 6 \, m_l^{(\mathrm{phys})}$ and for a few values of M/m_s. Straight lines refer to the continuum extrapolations obtained by fitting determinations obtained for the 3 finest lattice spacings with a linear function in a^2. Full points in $a = 0$ represent the corresponding continuum extrapolations. Right panel: continuum limits of $\chi_{\mathrm{SP}}^{1/4}$ obtained from spectral projectors at $m_l = 6 \, m_l^{(\mathrm{phys})}$ for several values of M/m_s. The shaded area represents our final result for the continuum limit of χ_{SP}.*
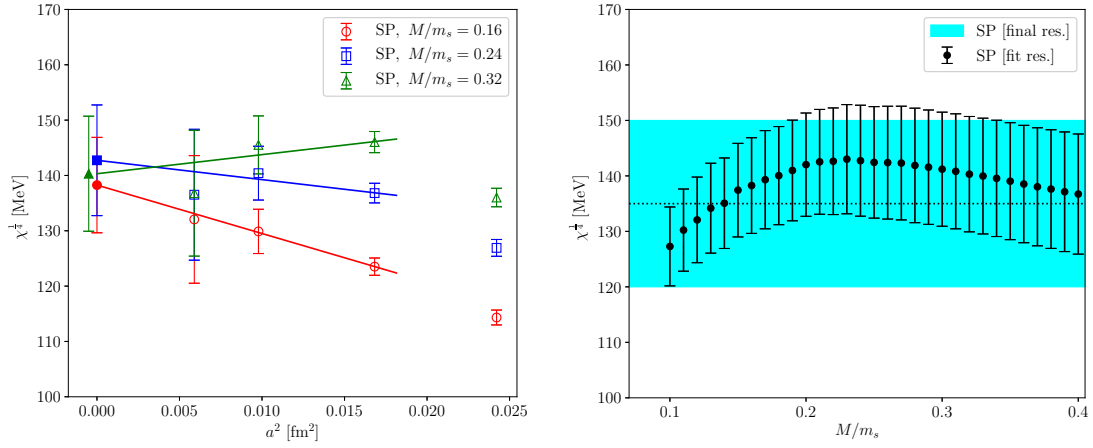
Figure 19: *Left panel: comparison of continuum limit extrapolations of $\chi_{\rm SP}^{1/4}(M/m_s)$ for $m_l = 9\ m_l^{\rm (phys)}$ and for a few values of M/m_s. Straight lines refer to the continuum extrapolations obtained by fitting determinations obtained for the 3 finest lattice spacings with a linear function in a^2. Full points in $a = 0$ represent the corresponding continuum extrapolations. Right panel: continuum limits of $\chi_{\rm SP}^{1/4}$ obtained from spectral projectors at $m_l = 9\ m_l^{\rm (phys)}$ for several values of M/m_s. The shaded area represents our final result for the continuum limit of $\chi_{\rm SP}$.*

References

[1] J. Gasser and H. Leutwyler, *Chiral Perturbation Theory to One Loop*, *Annals Phys.* **158** (1984) 142.

[2] J. Gasser and H. Leutwyler, *Chiral Perturbation Theory: Expansions in the Mass of the Strange Quark*, *Nucl. Phys. B* **250** (1985) 465.

[3] PARTICLE DATA GROUP collaboration, R. L. Workman and Others, *Review of Particle Physics*, *PTEP* **2022** (2022) 083C01.

[4] C. Bonati, M. D'Elia, M. Mariti, G. Martinelli, M. Mesiti, F. Negro et al., *Axion phenomenology and θ-dependence from $N_f = 2 + 1$ lattice QCD*, *JHEP* **03** (2016) 155 [1512.06746].

[5] P. Petreczky, H.-P. Schadler and S. Sharma, *The topological susceptibility in finite temperature QCD and axion cosmology*, *Phys. Lett. B* **762** (2016) 498 [1606.03145].

[6] S. Borsanyi et al., *Calculation of the axion mass based on high-temperature lattice quantum chromodynamics*, *Nature* **539** (2016) 69 [1606.07494].

[7] J. Frison, R. Kitano, H. Matsufuru, S. Mori and N. Yamada, *Topological susceptibility at high temperature on the lattice*, *JHEP* **09** (2016) 021 [1606.07175].

[8] C. Alexandrou, A. Athenodorou, K. Cichy, M. Constantinou, D. P. Horkel, K. Jansen et al., *Topological susceptibility from twisted mass fermions using spectral projectors and the gradient flow*, *Phys. Rev. D* **97** (2018) 074503 [1709.06596].

[9] C. Bonati, M. D'Elia, G. Martinelli, F. Negro, F. Sanfilippo and A. Todaro, *Topology in full QCD at high temperature: a multicanonical approach*, *JHEP* **11** (2018) 170 [1807.07954].

[10] A. Athenodorou, C. Bonanno, C. Bonati, G. Clemente, F. D'Angelo, M. D'Elia et al., *Topological susceptibility of $N_f = 2 + 1$ QCD from staggered fermions spectral projectors at high temperatures*, *JHEP* **10** (2022) 197 [2208.08921].

[11] ETM collaboration, R. Baron et al., *Light Meson Physics from Maximally Twisted Mass Lattice QCD*, *JHEP* **08** (2010) 097 [0911.5061].

[12] K. Cichy, E. Garcia-Ramos and K. Jansen, *Chiral condensate from the twisted mass Dirac operator spectrum*, *JHEP* **10** (2013) 175 [1303.1954].

[13] B. B. Brandt, A. Jüttner and H. Wittig, *The pion vector form factor from lattice QCD and NNLO chiral perturbation theory*, *JHEP* **11** (2013) 034 [1306.2916].

[14] G. P. Engel, L. Giusti, S. Lottini and R. Sommer, *Spectral density of the Dirac operator in two-flavor QCD*, *Phys. Rev. D* **91** (2015) 054505 [1411.6386].

[15] A. Bazavov et al., *Staggered chiral perturbation theory in the two-flavor case and SU(2) analysis of the MILC data*, *PoS* **LATTICE2010** (2010) 083 [1011.1792].

[16] S. Borsanyi, S. Durr, Z. Fodor, S. Krieg, A. Schafer, E. E. Scholz et al., *SU(2) chiral perturbation theory low-energy constants from 2+1 flavor staggered lattice simulations*, *Phys. Rev. D* **88** (2013) 014513 [1205.0788].

[17] BUDAPEST-MARSEILLE-WUPPERTAL collaboration, S. Dürr et al., *Lattice QCD at the physical point meets SU(2) chiral perturbation theory*, *Phys. Rev. D* **90** (2014) 114504 [1310.3626].

[18] P. A. Boyle et al., *Low energy constants of SU(2) partially quenched chiral perturbation theory from N_f=2+1 domain wall QCD*, *Phys. Rev. D* **93** (2016) 054502 [1511.01950].

[19] G. Cossu, H. Fukaya, S. Hashimoto, T. Kaneko and J.-I. Noaki, *Stochastic calculation of the Dirac spectrum on the lattice and a determination of chiral condensate in 2+1-flavor QCD*, *PTEP* **2016** (2016) 093B06 [1607.01099].

[20] JLQCD collaboration, S. Aoki, G. Cossu, H. Fukaya, S. Hashimoto and T. Kaneko, *Topological susceptibility of QCD with dynamical Möbius domain-wall fermions*, *PTEP* **2018** (2018) 043B07 [1705.10906].

[21] R. Narayanan and H. Neuberger, *Chiral symmetry breaking at large N_c*, *Nucl. Phys. B* **696** (2004) 107 [hep-lat/0405025].

[22] G. S. Bali, F. Bursa, L. Castagnini, S. Collins, L. Del Debbio, B. Lucini et al., *Mesons in large-N QCD*, *JHEP* **06** (2013) 071 [1304.4437].

[23] P. Hernández, C. Pena and F. Romero-López, *Large N_c scaling of meson masses and decay constants*, *Eur. Phys. J. C* **79** (2019) 865 [1907.11511].

[24] M. G. Pérez, A. González-Arroyo and M. Okawa, *Meson spectrum in the large N limit*, *JHEP* **04** (2021) 230 [2011.13061].

[25] FLAVOUR LATTICE AVERAGING GROUP (FLAG) collaboration, Y. Aoki et al., *FLAG Review 2021*, *Eur. Phys. J. C* **82** (2022) 869 [2111.09849].

[26] L. Giusti and M. Lüscher, *Chiral symmetry breaking and the Banks-Casher relation in lattice QCD with Wilson quarks*, *JHEP* **03** (2009) 013 [0812.3638].

[27] M. Lüscher and F. Palombi, *Universality of the topological susceptibility in the $SU(3)$ gauge theory*, *JHEP* **09** (2010) 110 [1008.0732].

[28] C. Morningstar and M. J. Peardon, *Analytic smearing of SU(3) link variables in lattice QCD*, *Phys. Rev. D* **69** (2004) 054501 [`hep-lat/0311018`].

[29] M. A. Clark and A. D. Kennedy, *Accelerating dynamical fermion computations using the rational hybrid Monte Carlo (RHMC) algorithm with multiple pseudofermion fields*, *Phys. Rev. Lett.* **98** (2007) 051601 [`hep-lat/0608015`].

[30] M. A. Clark and A. D. Kennedy, *Accelerating Staggered Fermion Dynamics with the Rational Hybrid Monte Carlo (RHMC) Algorithm*, *Phys. Rev. D* **75** (2007) 011502 [`hep-lat/0610047`].

[31] Y. Aoki, S. Borsanyi, S. Durr, Z. Fodor, S. D. Katz, S. Krieg et al., *The QCD transition temperature: results with physical masses in the continuum limit II.*, *JHEP* **06** (2009) 088 [`0903.4155`].

[32] S. Borsanyi, G. Endrodi, Z. Fodor, A. Jakovac, S. D. Katz, S. Krieg et al., *The QCD equation of state with dynamical quarks*, *JHEP* **11** (2010) 077 [`1007.2580`].

[33] S. Borsanyi, Z. Fodor, C. Hoelbling, S. D. Katz, S. Krieg and K. K. Szabo, *Full result for the QCD equation of state with 2+1 flavors*, *Phys. Lett. B* **730** (2014) 99 [`1309.5258`].

[34] BMW collaboration, S. Borsanyi et al., *High-precision scale setting in lattice QCD*, *JHEP* **09** (2012) 010 [`1203.4469`].

[35] T. Banks and A. Casher, *Chiral Symmetry Breaking in Confining Theories*, *Nucl. Phys. B* **169** (1980) 103.

[36] C. Bonanno, G. Clemente, M. D'Elia and F. Sanfilippo, *Topology via spectral projectors with staggered fermions*, *JHEP* **10** (2019) 187 [`1908.11832`].

[37] MILC collaboration, A. Bazavov et al., *Nonperturbative QCD Simulations with 2+1 Flavors of Improved Staggered Quarks*, *Rev. Mod. Phys.* **82** (2010) 1349 [`0903.3598`].

[38] B. Berg, *Dislocations and Topological Background in the Lattice O(3) σ Model*, *Phys. Lett. B* **104** (1981) 475.

[39] Y. Iwasaki and T. Yoshie, *Instantons and Topological Charge in Lattice Gauge Theory*, *Phys. Lett. B* **131** (1983) 159.

[40] S. Itoh, Y. Iwasaki and T. Yoshie, *Stability of Instantons on the Lattice and the Renormalized Trajectory*, *Phys. Lett. B* **147** (1984) 141.

[41] M. Teper, *Instantons in the Quantized SU(2) Vacuum: A Lattice Monte Carlo Investigation*, *Phys. Lett. B* **162** (1985) 357.

[42] E.-M. Ilgenfritz, M. Laursen, G. Schierholz, M. Müller-Preussker and H. Schiller, *First Evidence for the Existence of Instantons in the Quantized SU(2) Lattice Vacuum*, *Nucl. Phys. B* **268** (1986) 693.

[43] M. Campostrini, A. Di Giacomo, H. Panagopoulos and E. Vicari, *Topological Charge, Renormalization and Cooling on the Lattice*, *Nucl. Phys. B* **329** (1990) 683.

[44] B. Alles, L. Cosmai, M. D'Elia and A. Papa, *Topology in 2D CP^{N-1} models on the lattice: A Critical comparison of different cooling techniques*, *Phys. Rev. D* **62** (2000) 094507 [`hep-lat/0001027`].

[45] C. Bonati and M. D'Elia, *Comparison of the gradient flow with cooling in SU(3) pure gauge theory*, *Phys. Rev. D* **D89** (2014) 105005 [`1401.2441`].

[46] C. Alexandrou, A. Athenodorou and K. Jansen, *Topological charge using cooling and the gradient flow*, *Phys. Rev. D* **92** (2015) 125014 [`1509.04259`].

[47] M. Lüscher, *Trivializing maps, the Wilson flow and the HMC algorithm*, *Commun. Math. Phys.* **293** (2010) 899 [`0907.5491`].

[48] M. Lüscher, *Properties and uses of the Wilson flow in lattice QCD*, *JHEP* **08** (2010) 071 [`1006.4518`].

[49] L. Del Debbio, H. Panagopoulos and E. Vicari, *theta dependence of $SU(N)$ gauge theories*, *JHEP* **08** (2002) 044 [`hep-th/0204125`].

[50] C. Bonati, M. D'Elia and A. Scapellato, *θ dependence in $SU(3)$ Yang-Mills theory from analytic continuation*, *Phys. Rev. D* **93** (2016) 025028 [`1512.01544`].

[51] ETM collaboration, K. Cichy, E. Garcia-Ramos, K. Jansen, K. Ottnad and C. Urbach, *Non-perturbative Test of the Witten-Veneziano Formula from Lattice QCD*, *JHEP* **09** (2015) 020 [`1504.07954`].

[52] C. T. H. Davies, C. McNeile, K. Y. Wong, E. Follana, R. Horgan, K. Hornbostel et al., *Precise Charm to Strange Mass Ratio and Light Quark Masses from Full Lattice QCD*, *Phys. Rev. Lett.* **104** (2010) 132003 [`0910.3102`].